Selective Regional Correlation for Pattern Recognition

Ervin Sejdić, *Student Member, IEEE*, and Jin Jiang, *Senior Member, IEEE*

***Abstract*—In this paper, a novel correlation-based pattern classifier that relies on the analysis of time–frequency decomposition of a template and signals is proposed. Significant improvements in resolution and accuracy are obtained using this new classifier when compared to a conventional correlation-based one. The short-time Fourier transform, continuous wavelet transform, and S-transform are considered in the time–frequency decomposition process. To evaluate the performance of the proposed scheme, numerical studies are performed on a set of synthetic test signals, and excellent results have been obtained. This paper also presents an illustrative example where two types of heart sounds are classified. The classification error percentage for the heart sounds using the new classifier is only 6.670% as compared to 56.67% when a general correlation-based classifier is used.**

***Index Terms*—Correlation, heart sounds, pattern recognition, selective regional correlation (SRC), time–frequency transformations.**

I. Introduction

AUTOMATIC recognition and pattern matching for signals bearing particular characteristics buried in other signals or noise can be a difficult task. If a correlation-type scheme is used, the corrupting signals/noise can affect the accuracy of pattern matching and subsequently lead to errors in classification [1], which is due to the fact that the corrupting signals may also bear some resemblance to the template being matched. This is particularly true if the pattern of interest is a transient signal in a nonstationary environment. Even though correlation is a very powerful tool that has been used extensively in many applications [2], it has limitations of its own. Traditional time-domain correlation-based pattern recognition methods do not fully utilize the frequency characteristics of the template and the signal being analyzed. It is important to point out that if a template has bandlimited characteristics, a significant improvement in the performance of pattern recognition can be readily made by relatively simple preprocessing of the signal and the template in the time–frequency domain. Such preprocessing can effectively separate the intertwined time-domain features of the signal, allowing the important characteristics to be exposed in the time–frequency domain for more effective pattern matching.

Manuscript received November 12, 2003; revised April 5, 2004, October 4, 2004, April 6, 2005, and August 17, 2005. This work was supported by the Natural Sciences and Engineering Research Council of Canada. This paper was recommended by Associate Editor W. Pedrycz.

The authors are with the Department of Electrical and Computer Engineering, The University of Western Ontario, London, ON N6A 5B9, Canada (e-mail: esejdic@ieee.org; jjiang@eng.uwo.ca).

Digital Object Identifier 10.1109/TSMCA.2006.886333

A novel scheme for improving the performance of correlation-based pattern recognition for bandlimited nonstationary signals is developed in this paper based on time–frequency analysis tools. The preprocessing is carried out by converting a one-dimensional (1-D) time-domain signal into a two-dimensional (2-D) time–frequency domain representation. Thus, the true time–frequency composition of the signal can be clearly revealed. This allows correlation-based pattern matching to be conducted only in selected regions in the time–frequency domain. The newly developed technique is referred to as selective regional correlation (SRC). To emphasize the potential of this method and its effectiveness, different time–frequency transforms, i.e., short-time Fourier transform (STFT) [3], [4], continuous wavelet transform (CWT) [5]–[8], and the S-transform (ST) [9] have been used as the tools for such preprocessing. The performance under these tools has also been compared.

The proposed scheme is tested using a set of synthetic test signals, which contain short-duration transients. Using these test signals, the SRC is evaluated and compared to general correlation. The results have shown that the SRC enhances the resolution and accuracy for classification of transient signals. The technique proposed herein may be of significance in many applications where correlation-based techniques have been used traditionally, such as communications, statistical signal processing, and time-series analysis. As an illustrative example, the developed scheme has been evaluated by applying it to the classification of heart sounds to detect pathological states.

This paper is organized as follows. In Section II, the concept of SRC is presented in comparison with the traditional correlation in the context of pattern recognition. The detailed theoretical development of the SRC is covered in Section III. Section IV illustrates the performance of the proposed scheme, and in Section V, the scheme is applied to heart-sound analysis, in particular, to distinguish the presence of opening snaps from third heart sounds. General remarks regarding the proposed scheme and its limitations are presented in Section V-C. Finally, conclusions are drawn in Section VI.

II. Correlation-Based Pattern Recognition in Time–Frequency Domain

Pattern recognition is a very powerful tool in automated data analysis and decision making. Its applications can be found in speech processing [10], fault diagnosis [11], fingerprint matching [12], DNA classification [13], and satellite image processing [14], to name a few. The basic idea of a correlation-based pattern recognition scheme is to correlate the signal being

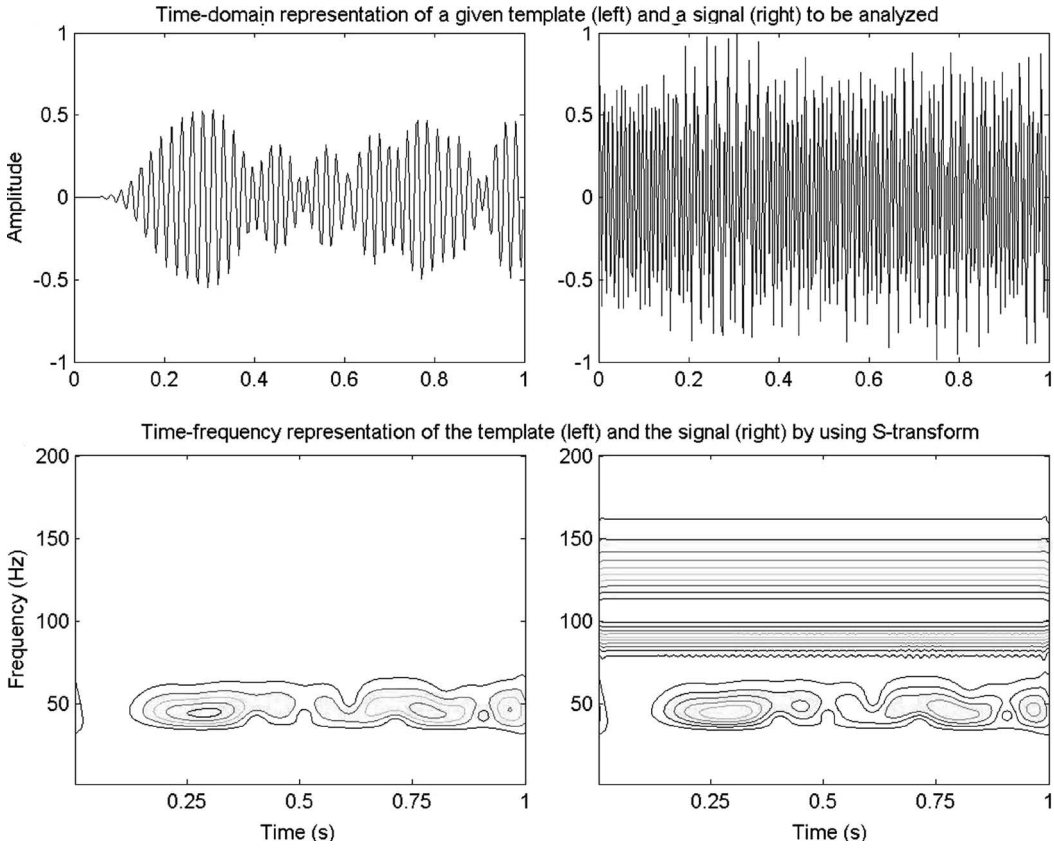

Fig. 1. Time-domain and time–frequency domain representations of (left) a template and (right) a signal.

analyzed with a known template [15], [16] and make decisions based on the magnitude of the correlation coefficients. The process of correlation is essentially to determine the degree of similarity between the signal being analyzed and the template. The outcome of the correlation can be expressed in terms of an absolute value of the correlation coefficient between zero and one. The value of zero implies that the signal has no resemblance (orthogonal) to the template at all, while the value of unity means that the signal is identical to the template possibly with a phase shift or a scaling factor in amplitude at the most. In a practical situation, one would seldom achieve zero or one, as there are always some disturbances or noise in the signal being analyzed. For any value between zero and one, a decision threshold has to be established for proper classification.

Even though the idea of a correlation-based method is straightforward, it does have some limitations. The main drawback can be traced to the composition of the signal and the template. The desirable portion of the signal could be buried in noise or other nuisance signals. A direct correlation of the signal with the template may produce a low correlation coefficient even if the signal may contain the same pattern as that in the template, which could lead to an erroneous decision. This situation can best be illustrated through the following example.

Consider a template and a signal being analyzed as illustrated in the top two graphs of Fig. 1. By visual inspection, it is very difficult to convince anyone that there are any similarities between them. If a correlation is performed between them, the peak correlation coefficient of 0.3066 supports the visual inspection. However, the bottom graphs of Fig. 1 show the time–frequency representation (TFR) of the template as well as that of the signal. Clearly, the signal does contain a component very similar to that of the template in the frequency band between 40 and 60 Hz. However, this component has completely been buried in another signal when observed in the time domain. If the signal in the frequency band between 40 to 60 Hz is selected to perform the correlation with the template, the correlation coefficient becomes as high as 0.9990.

Even though this is an artificial example, it does illustrate the point that a certain type of signal preprocessing may be useful to achieve improved performance in pattern recognition. Such preprocessing becomes possible when time–frequency domain signal decomposition techniques are used.

III. Proposed Scheme

The decision of a correlation-based pattern classifier depends on the output value of the correlator, and thus, its performance will be directly related to the quality of the correlation process. If the pattern of interest is present in the signal being analyzed, the correlator should produce a large correlation coefficient; otherwise, it should result in a small one. The difference between these two values is known as the resolution of the pattern classifier. In order to improve the quality of pattern recognition, this resolution can be enhanced further by increasing it when the signal matches the template, and reducing it when they do not. The SRC is based precisely on this philosophy with the help of time–frequency domain signal preprocessing techniques.

A. Problem Statement

The problem to be investigated in this paper can be stated as follows. For a given bandlimited template $p(t)$ and a signal $s(t)$ design a preprocessing scheme, such that when $s(t)$ matches $p(t)$, the peak value of the correlation coefficient is further increased, otherwise decreased. In other words, the problem dealt with herein is to design a signal preprocessor to enhance the resolution of the pattern classifier by improving the quality of correlation using the time–frequency domain decomposition techniques.

B. SRC

The essence of the proposed scheme, as mentioned previously, is to represent a 1-D time-domain signal in a 2-D TFR to reveal its true characteristics for more accurate pattern matching. The linear time–frequency transform can be defined as an inner product of the template $p(t)$ or the signal $s(t)$ with a function $\phi_{\tau,\gamma} \in \mathbf{L}^2(R)$ (sometimes known as the time–frequency atom) that is well concentrated in time and frequency [6]. Therefore, the following lemmas can be formulated.

Lemma 1: If the template is represented by $p(t)$, its time–frequency transform can be represented as

$$Tp(\tau,\gamma) = \int_{-\infty}^{\infty} p(t)\phi_{\tau,\gamma}(t)dt \tag{1}$$

and

$$Tp(\tau,\gamma) \equiv 0 \quad \forall \quad \tau \notin [\tau_1,\tau_2] \quad \gamma \notin [\gamma_1,\gamma_2] \tag{2}$$

where τ_1 and τ_2 are the lower and the upper limits of the time band and γ_1 and γ_2 are the lower and the upper limits of the frequency band.

Lemma 2: For a finite-duration signal, $s(t)t \in [t_1,t_2]$, its TFR can be obtained by (1) with $p(t)$ substituted by $s(t)$ and represented by $Ts(\tau,\gamma)$. Thus, the following signal decomposition is in order:

$$Ts(\tau,\gamma) = Ts_1(\tau,\gamma) \cup Ts_2(\tau,\gamma) \tag{3}$$

where

$$Ts_1(\tau,\gamma) = Ts(\tau,\gamma) \quad \tau \in [\tau_1,\tau_2] \quad \gamma \in [\gamma_1,\gamma_2] \tag{4}$$

and

$$Ts_2(\tau,\gamma) = \overline{Ts(\tau,\gamma) \cap Ts_1(\tau,\gamma)}. \tag{5}$$

In other words, $Ts_1(\tau,\gamma)$ represents the portion of the signal in the time and frequency range of the template, and $Ts_2(\tau,\gamma)$ is its complement, representing the remaining signal elements.

To effectively obtain $Ts_1(\tau,\gamma)$ from $Ts(\tau,\gamma)$, different 2-D windows can be used. However, when window functions are used to extract the relevant portion of the signal, they may also introduce additional transients when transforming back to time domain. Care should be taken when extracting $Ts_1(\tau,\gamma)$ from $Ts(\tau,\gamma)$ to minimize the edge effects by using proper window functions.

Lemma 3: If a 2-D window is represented in the time–frequency domain as: $W(\tau,\gamma) \quad \forall \quad \tau \in [\tau_1,\tau_2]$ and $\gamma \in [\gamma_1,\gamma_2]$, then

$$Ts_1(\tau,\gamma) = Ts(\tau,\gamma)\cdot W(\tau,\gamma) \;\; \tau \in [\tau_1,\tau_2] \quad \gamma \in [\gamma_1,\gamma_2]. \tag{6}$$

An elliptic type of window is chosen in this paper for the least amount of edge effect. A Gaussian elliptic window is a window whose boundaries are defined by an ellipse [17], while weights on the points inside the ellipse are assigned according to a Gaussian distribution. A Gaussian elliptic window can be expressed as

$$W_{\mathrm{g}}(\tau,\gamma) = \begin{cases} \frac{1}{2\pi\sigma_\tau\sigma_\gamma} e^{-\frac{\tau^2}{2\sigma_\tau^2}-\frac{\gamma^2}{2\sigma_\gamma^2}}, & \forall \quad \tau,\gamma \in \Omega \\ 0, & \text{otherwise} \end{cases} \tag{7}$$

where the support region is $\Omega = \{(\tau,\gamma) : \tau \in [\tau_1,\tau_2], \gamma \in [\gamma_1,\gamma_2],\ (\tau/a)^2 + (\gamma/b)^2 = 1\}$. The constants a and b represent half of the major and minor axes, respectively. σ_τ^2 and σ_γ^2 represent the variances in time and frequency domain, respectively, and collectively, they determine the shape of this 2-D window.

Corollary 1: Based on Lemma 2 and Lemma 3, the corresponding time-domain signal $s(t)$ can be represented as

$$s(t) = s_1(t) + s_2(t) \tag{8}$$

where $s_1(t)$ and $s_2(t)$ are the inverse time–frequency transforms of $Ts_1(\tau,\gamma)$ and $Ts_2(\tau,\gamma)$, respectively, defined by

$$s_i(t) = \int_{-\infty}^{\infty}\int_{-\infty}^{\infty} Ts_i(\tau,\gamma)K(\tau,\gamma,t)d\tau d\gamma, \qquad i = 1,2 \tag{9}$$

and $K(\tau,\gamma,t)$ is a kernel used in the inverse transform.

Theorem 1: If the pattern similar to that of the template $p(t)$ is present in the signal $s(t)$, then the following is true:

$$\max\left[|\mathrm{corr}\,(s_1(t),p(t))|\right] > \max\left[|\mathrm{corr}\,(s(t),p(t))|\right] \tag{10}$$

where $\max[|\mathrm{corr}(x(t),y(t))|]$ is defined as

$$\max\left[|\mathrm{corr}\,(x(t),y(t))|\right] = \max_{\tau}\left[\left|\frac{\int_{-\infty}^{\infty} x(t)y(t+\tau)dt}{\sqrt{\int_{-\infty}^{\infty} x(t)^2dt}\sqrt{\int_{-\infty}^{\infty} y(t)^2dt}}\right|\right] \tag{11}$$

and $x(t)$ and $y(t)$ are zero-mean signals. The proof of Theorem 1 is given in Appendix I.

So far, only one scenario has been considered, i.e., the signal either contains the template, or not. Theorem 1 proves that if the signal contains the template, the SRC will result in the largest peak correlation coefficient. The concept of the SRC is also applicable to the multiple-template case, but certain precautions

must be taken when selecting the templates. The most important consideration is that the templates must be mutually exclusive.

Assume that $p_1(t), \ldots, p_m(t)$ are the templates with the TFR $Tp_1(\tau,\gamma), \ldots, Tp_m(\tau,\gamma)$, respectively. The following lemma is in order.

Lemma 4: If the TFRs of the templates, $Tp_1(\tau,\gamma)$, $Tp_2(\tau,\gamma), \ldots, Tp_m(\tau,\gamma)$ are disjoint sets, i.e.,

$$Tp_1(\tau,\gamma) \cap Tp_2(\tau,\gamma) \cap Tp_3(\tau,\gamma) \cap \cdots \cap Tp_m(\tau,\gamma) = \emptyset \tag{12}$$

then a template $p_i(t)$ can be found by multiplying a time–frequency decomposition of the template $Tp_i(\tau,\gamma)$ with a 2-D window, $W_i(\tau,\gamma)$ with appropriate time and frequency band limits, and inverting back to the time domain

$$p_i(t) = \int_{-\infty}^{\infty}\int_{-\infty}^{\infty} Tp_i(\tau,\gamma) W_i(\tau,\gamma) K(\tau,\gamma,t) d\tau d\gamma. \tag{13}$$

Lemma 5: If the TFRs of the templates, $Tp_1(\tau,\gamma)$, $Tp_2(\tau,\gamma) \cdots Tp_m(\tau,\gamma)$ are not disjoint sets, i.e.,

$$Tp_k(\tau,\gamma) \cap Tp_l(\tau,\gamma) \neq \emptyset, \quad \text{for} \quad k \neq l \tag{14}$$

for some k and l, it is necessary to introduce a mutually exclusive template in order to reduce the peak correlation coefficient when the signal does not match the template. This exclusivity is introduced in the time–frequency domain as

$$Tp'_k(\tau,\gamma) = Tp_k(\tau,\gamma) - (Tp_k(\tau,\gamma) \cap Tp_l(\tau,\gamma)) \tag{15}$$

and the corresponding template in the time domain will be

$$p'_k(t) = \int_{-\infty}^{\infty}\int_{-\infty}^{\infty} Tp'_k(\tau,\gamma) W_k(\tau,\gamma) K(\tau,\gamma,t) d\tau d\gamma. \tag{16}$$

The mutual exclusivity of the templates stated in Lemma 4 and Lemma 5 is the main reason why the SRC is a superior pattern-matching technique to the general correlation-based approach. The exclusivity of the templates is only possible by introducing the redundant representation of the signal such as TFR.

Corollary 2: Based on Lemma 4 and Lemma 5, it can be stated that any template is a sum of mutually exclusive terms, $p'(t)$, and $p''(t)$. That is

$$p(t) = p'(t) + p''(t) \tag{17}$$

where $p''(t)$ would be zero for disjoint templates. In addition, it is necessary to have the following constraint:

$$\int_{-\infty}^{\infty}\int_{-\infty}^{\infty} |Tp'(\tau,\gamma)|\, d\tau d\gamma \gg \int_{-\infty}^{\infty}\int_{-\infty}^{\infty} |Tp''(\tau,\gamma)|\, d\tau d\gamma. \tag{18}$$

Theorem 2: If the signal $z(t)$ does not contain the template $p(t)$, then the SRC using $p'(t)$ will produce a smaller correlation coefficient, namely

$$\max\left[|\mathrm{corr}\left(z(t), p(t)\right)|\right] > \max\left[|\mathrm{corr}\left(z(t), p'(t)\right)|\right] \tag{19}$$

where $\max[|\mathrm{corr}(x(t), y(t))|]$ is as defined in (11).

Theorem 2 states that the SRC can reduce the peak correlation coefficient when the signal does not contain the template. The proof for this theorem can be found in Appendix II.

The flowchart of the algorithm is presented in Fig. 2 as a brief summary of the procedure.

IV. Performance Evaluation of SRC Using Synthetic Test Signals

In this section, the performance of the proposed scheme is examined using a set of synthetic test signals. The goal is to examine how the SRC performs in comparison to general correlation. The analysis starts with a simple case with one template and progresses to more complicated cases with multiple templates.

In the analysis, three different time–frequency transforms are used: STFT, CWT, and ST. The difference between these three transforms is the time–frequency atom $\phi_{\tau,\gamma}(t)$ in (1). An STFT is defined as a window g which is translated by τ and modulated by γ [3], [6]

$$\phi_{\tau,\gamma}(t) = g_{\tau,\gamma}(t) = e^{-j\gamma t} g(t-\tau). \tag{20}$$

A CWT is defined as a mother wavelet ψ with dilation by γ and translation by τ [5]–[8]

$$\phi_{\tau,\gamma}(t) = \psi_{\tau,\gamma}(t) = \frac{1}{\sqrt{\gamma}} \psi\left(\frac{t-\tau}{\gamma}\right). \tag{21}$$

An ST combines STFT and CWT using a Gaussian window which is translated by τ, dilated and modulated by γ [9], [18]–[20]

$$\phi_{\tau,\gamma}(t) = g_{\tau,\gamma}(t) = e^{-j\gamma t} g\left(\frac{t-\tau}{\gamma}\right). \tag{22}$$

Clearly, the ST can be viewed from two different perspectives, an STFT with a variable window length [9], [20], or as a special type of CWT with a Gaussian mother wavelet multiplied by a phase factor [9], [20]

$$\mathrm{ST}(\tau,\gamma) = e^{-j2\pi\gamma\tau} \mathrm{CWT}(\tau,\gamma). \tag{23}$$

The goal of the numerical study on synthetic signals is to examine the performance of the SRC classifier for different patterns. The robustness with respect to the specific type of time–frequency transforms and slight variations in patterns are also examined. In order to evaluate the resolution, two states, in which correlation coefficients ρ_k can belong to, are used: ρ_{M} or ρ_{NM}. ρ_{M} represents the situation where the signal contains the template as specified, while ρ_{NM} represents the situation where the signal does not contain the template.

The performance can be measured by calculating the resolution between the correlation coefficients in these two situations. The resolution of the SRC scheme φ is defined as

$$\varphi = \rho_{\mathrm{M}} - \rho_{\mathrm{NM}}. \tag{24}$$

To show that the SRC improves the accuracy of the classifier, the number of correct classifications (CC), and misclassifications (MC) for both the general correlation and the SRC

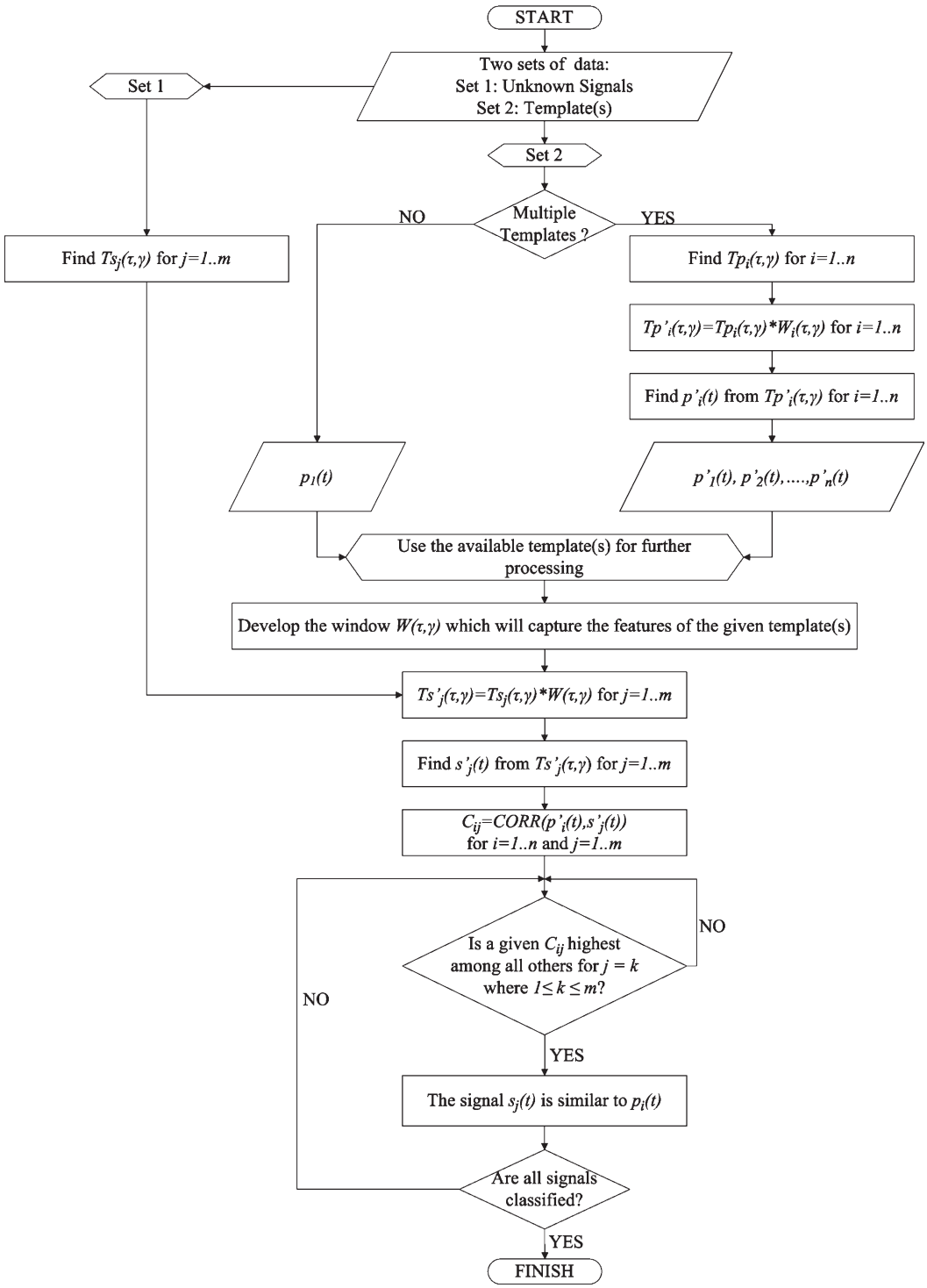

Fig. 2. Flowchart of the SRC algorithm.

have been recorded. Based on these two numbers, the error percentage (EP) can be calculated as follows:

$$\text{EP} = \frac{\text{MC}}{\text{MC} + \text{CC}} * 100\%. \tag{25}$$

A. Templates and Signals Used in Evaluation

The design of the template and the signal for the single template case is rather straightforward. For a single template case, it is desired to show that if the signal is preprocessed prior to correlation, a significantly better result can be obtained. For this purpose, the template $p(t)$ and the signal $s(t)$ are defined as follows:

$$p(t) = \begin{cases} \sin(2\pi 150t), & 0.2 \le t \le 0.6 \\ 0, & \text{otherwise} \end{cases} \tag{26}$$

$$s(t) = \begin{cases} \sin(2\pi 30t) + \sin(2\pi 150t), & 0.2 \le t \le 0.6 \\ \sin(2\pi 30t), & \text{otherwise} \end{cases} \tag{27}$$

where $t \in [0, 1]$.

The design process of the synthetic templates and the signals for dual/multiple-template case is more complex. Most of the real-world patterns are not limited only to a single frequency, but rather are a sum of transients with different frequencies. Very often, these frequencies are not constant; they can vary with time, but often within a certain frequency band. Measurement noise may further contaminate the signals. Therefore, in order to be closer to practical conditions, the following rules are used while designing the templates and the signals.

1) Each template will consist of four unique transients of different frequencies, where the minimum and the maximum frequencies among those four represent the boundaries.
2) Unprocessed template signals $p_1(t), \ldots, p_m(t)$ will have some overlapping areas in the time–frequency domain, which will be removed at the preprocessing stage.
3) Signals will have their transient frequencies assigned according to the boundary rules mentioned above.
4) Each signal also contains additional transients which simulate contamination signals.

Based on these rules, the following templates and signals have been used in the dual-template case:

$$p_1(t) = \begin{cases} p_o(t) + \sin(2\pi 95t) + \sin(2\pi 102t) \\ \quad + \sin(2\pi 105t) + \sin(2\pi 110t), \\ \qquad 0.4 \le t \le 0.6 \\ p_o(t), \qquad \text{otherwise} \end{cases} \tag{28}$$

$$p_2(t) = \begin{cases} p_o(t) + \sin(2\pi 60t) + \sin(2\pi 67t) \\ \quad + \sin(2\pi 70t) + \sin(2\pi 75t), \\ \qquad 0.58 \le t \le 0.74 \\ p_o(t), \qquad \text{otherwise} \end{cases} \tag{29}$$

$$s_{1_i}(t) = \begin{cases} p_o(t) + \sum_{k=1}^{k=6} \sin\left(\lfloor 2\pi 250R \rfloor t\right), \\ \qquad 0.04 + \frac{\lfloor 30R \rfloor}{500} \le t \le 0.26 + \frac{\lfloor 20R \rfloor}{500} \\ p_o(t) + \sum_{n=1}^{n=4} \sin\left(2\pi(95 + \lfloor 15R \rfloor)t\right), \\ \qquad 0.40 + \frac{\lfloor 20R \rfloor}{500} \le t \le 0.60 + \frac{\lfloor 20R \rfloor}{500} \\ p_o(t) + \sum_{k=1}^{k=6} \sin\left(\lfloor 2\pi 250R \rfloor t\right), \\ \qquad 0.84 + \frac{\lfloor 20R \rfloor}{500} \le t \le 0.90 + \frac{\lfloor 25R \rfloor}{500} \\ p_o(t), \quad \text{otherwise} \end{cases} \tag{30}$$

$$s_{2_i}(t) = \begin{cases} p_o(t) + \sum_{k=1}^{k=6} \sin\left(\lfloor 2\pi 250R \rfloor t\right), \\ \qquad 0.04 + \frac{\lfloor 30R \rfloor}{500} \le t \le 0.26 + \frac{\lfloor 20R \rfloor}{500} \\ p_o(t) + \sum_{n=1}^{n=4} \sin\left(2\pi(60 + \lfloor 15R \rfloor)t\right), \\ \qquad 0.58 + \frac{\lfloor 20R \rfloor}{500} \le t \le 0.74 + \frac{\lfloor 20R \rfloor}{500} \\ p_o(t) + \sum_{k=1}^{k=6} \sin\left(\lfloor 2\pi 250R \rfloor t\right), \\ \qquad 0.84 + \frac{\lfloor 20R \rfloor}{500} \le t \le 0.90 + \frac{\lfloor 25R \rfloor}{500} \\ p_o(t), \quad \text{otherwise} \end{cases} \tag{31}$$

where

$$p_o(t) = 0.8\left[\sin(2\pi 10t) + \sin(2\pi 15t) + \sin(2\pi 18t)\right] \tag{32}$$

and $R \sim |\mathcal{N}(0,1)|$ to simulate the uncertainties in the signals with $t \in [0,1]$. $\lfloor x \rfloor$ represents the greatest integer function which gives the largest integer less than or equal to x. As it can be seen from the definitions of the templates and the signals, they depict real-world signals quite well. These templates and signals are used in simulations, whose results are summarized in Section IV-C.

For the multiple-template case, the same rules are used while generating the templates and the signals

$$p_1(t) = \begin{cases} p_o(t) + \sin(2\pi 95t) + \sin(2\pi 100t) \\ \quad + \sin(2\pi 105t) + \sin(2\pi 110t), \\ \qquad 0.40 \le t \le 0.60 \\ p_o(t), \qquad \text{otherwise} \end{cases} \tag{33}$$

$$p_2(t) = \begin{cases} p_o(t) + \sin(2\pi 40t) + \sin(2\pi 47t) \\ \quad + \sin(2\pi 50t) + \sin(2\pi 55t), \\ \qquad 0.56 \le t \le 0.74 \\ p_o(t), \qquad \text{otherwise} \end{cases} \tag{34}$$

$$p_3(t) = \begin{cases} p_o(t) + \sin(2\pi 80t) + \sin(2\pi 85t) \\ \quad + \sin(2\pi 87t) + \sin(2\pi 90t), \\ \qquad 0.16 \le t \le 0.42 \\ p_o(t), \qquad \text{otherwise} \end{cases} \tag{35}$$

$$p_4(t) = \begin{cases} p_o(t) + \sin(2\pi 138t) + \sin(2\pi 143t) \\ \quad + \sin(2\pi 145t) + \sin(2\pi 150t), \\ \qquad 0.24 \le t \le 0.48 \\ p_o(t), \qquad \text{otherwise} \end{cases} \tag{36}$$

$$s_{1_i}(t) = \begin{cases} p_o(t) + \sum_{k=1}^{k=6} \sin\left(\lfloor 2\pi 250R \rfloor t\right), \\ \qquad 0.04 + \frac{\lfloor 20R \rfloor}{500} \le t \le 0.10 + \frac{\lfloor 20R \rfloor}{500} \\ p_o(t) + \sum_{n=1}^{n=4} \sin\left(2\pi(95 + \lfloor 15R \rfloor)t\right), \\ \qquad 0.40 + \frac{\lfloor 20R \rfloor}{500} \le t \le 0.60 + \frac{\lfloor 20R \rfloor}{500} \\ p_o(t) + \sum_{k=1}^{k=6} \sin\left(\lfloor 2\pi 250R \rfloor t\right), \\ \qquad 0.84 + \frac{\lfloor 20R \rfloor}{500} \le t \le 0.90 + \frac{\lfloor 25R \rfloor}{500} \\ p_o(t), \quad \text{otherwise} \end{cases} \tag{37}$$

$$s_{2_i}(t) = \begin{cases} p_o(t) + \sum_{k=1}^{k=6} \sin\left(\lfloor 2\pi 250R \rfloor t\right), \\ \qquad 0.04 + \frac{\lfloor 20R \rfloor}{500} \le t \le 0.10 + \frac{\lfloor 20R \rfloor}{500} \\ p_o(t) + \sum_{n=1}^{n=4} \sin\left(2\pi(40 + \lfloor 15R \rfloor)t\right), \\ \qquad 0.56 + \frac{\lfloor 20R \rfloor}{500} \le t \le 0.74 + \frac{\lfloor 20R \rfloor}{500} \\ p_o(t) + \sum_{k=1}^{k=6} \sin\left(\lfloor 2\pi 250R \rfloor t\right), \\ \qquad 0.84 + \frac{\lfloor 20R \rfloor}{500} \le t \le 0.90 + \frac{\lfloor 25R \rfloor}{500} \\ p_o(t), \quad \text{otherwise} \end{cases} \tag{38}$$

$$s_{3_i}(t) = \begin{cases} p_o(t) + \sum_{k=1}^{k=6} \sin\left(\lfloor 2\pi 250R \rfloor t\right), \\ \qquad 0.04 + \frac{\lfloor 20R \rfloor}{500} \le t \le 0.10 + \frac{\lfloor 20R \rfloor}{500} \\ p_o(t) + \sum_{n=1}^{n=4} \sin\left(2\pi(80 + \lfloor 10R \rfloor)t\right), \\ \qquad 0.16 + \frac{\lfloor 20R \rfloor}{500} \le t \le 0.42 + \frac{\lfloor 20R \rfloor}{500} \\ p_o(t) + \sum_{k=1}^{k=6} \sin\left(\lfloor 2\pi 250R \rfloor t\right), \\ \qquad 0.84 + \frac{\lfloor 20R \rfloor}{500} \le t \le 0.90 + \frac{\lfloor 25R \rfloor}{500} \\ p_o(t), \quad \text{otherwise} \end{cases} \tag{39}$$

$$s_{4_i}(t) = \begin{cases} p_o(t) + \sum_{k=1}^{k=6} \sin\left(\lfloor 2\pi 250R \rfloor t\right), \\ \qquad 0.04 + \frac{\lfloor 20R \rfloor}{500} \le t \le 0.10 + \frac{\lfloor 20R \rfloor}{500} \\ p_o(t) + \sum_{n=1}^{n=4} \sin\left(2\pi\left(138 + \lfloor 12R \rfloor\right)t\right), \\ \qquad 0.24 + \frac{\lfloor 20R \rfloor}{500} \le t \le 0.48 + \frac{\lfloor 20R \rfloor}{500} \\ p_o(t) + \sum_{k=1}^{k=6} \sin\left(\lfloor 2\pi 250R \rfloor t\right), \\ \qquad 0.84 + \frac{\lfloor 20R \rfloor}{500} \le t \le 0.90 + \frac{\lfloor 25R \rfloor}{500} \\ p_o(t), \quad \text{otherwise} \end{cases} \tag{40}$$

where R and t are as defined before and

$$p_o(t) = 5\left[\sin(2\pi 10t) + \sin(2\pi 15t) + \sin(2\pi 18t)\right]. \tag{41}$$

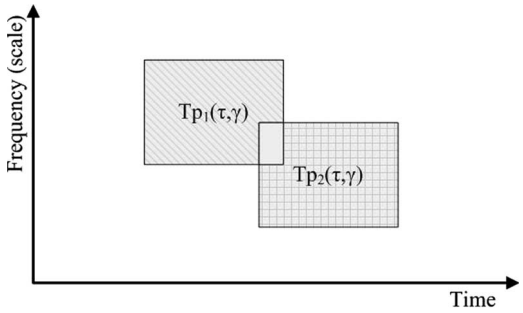

Fig. 3. Hypothetical dual-template position.

These signals and templates are used in Section IV-D for the multiple-template case.

B. Single Template

Based on the calculated TFR of $p(t)$ obtained according to (1), (22), and (26), the template occupies the following bands:

$$Tp(\tau,\gamma)=\{\,\Omega_{p_1}=\{(\tau,\gamma):\tau\in[0.2,0.6],\quad \gamma\in[120,210]\text{Hz}\} \tag{42}$$

such that the region of support Ω_{p_1} includes the band where the amplitude of TFRs $Tp(\tau,\gamma)$ is greater or equal to 1% of its maximum amplitude. Similarly, the calculated TFR of the signal $Ts(\tau,\gamma)$ occupies the following bands:

$$Ts(\tau,\gamma)=\begin{cases}\Omega_{s_1}=\{(\tau,\gamma):\tau\in[0.2,0.6],\gamma\in[120,210]\text{Hz}\}\\ \Omega_{s_2}=\{(\tau,\gamma):\tau\in[0,1],\gamma\in[24,45]\text{Hz}\}\,.\end{cases} \tag{43}$$

If general correlation between $p(t)$ and $s(t)$ is performed according to (11), the peak correlation coefficient ρ will be equal to 0.5345. From the TFRs of the template and the signal, it can be seen that there is a common term, namely the regions Ω_{p_1} and Ω_{s_1}. It is expected, based on Theorem 1, that the SRC would yield a larger correlation coefficient than general correlation. Therefore, based on time and frequency limits, the window $W_{\text{gs}}(\tau,\gamma)$ is designed to support the region Ω_{p_1}. The TFR of the signal $Ts(\tau,\gamma)$ is then multiplied by the window $W_{\text{gs}}(\tau,\gamma)$ to isolate the region of interest $Ts_1(\tau,\gamma)$. The inverse transform of the region $s_1(t)$ is obtained by (9).

Once the template $p(t)$ and the preprocessed signal $s_1(t)$ are obtained, the correlation process can be carried out using (11) with the two preprocessed signals. The peak correlation coefficient is equal to 0.9982.

C. Dual Templates

In the previous section, it has been shown that in the case of a single template, much improved results are obtained if the preprocessing of the signal and the template is carried out. A slightly more complicated situation occurs when the two templates have some overlaps as shown in Fig. 3. The two templates $p_1(t)$ and $p_2(t)$ have some similar features in the time–frequency domain, and these have to be decoupled.

It is assumed that it is desirable to differentiate among two types of signals that are similar in nature to the templates depicted in top two graphs of Fig. 4. They have the same low-frequency content, but the transients that occur in the templates represent two different phenomena as described by (28) and (29). The TFRs of the templates are obtained according to (1), (22), (28), and (29), and their main characteristics may be summarized by the following equations:

$$Tp_1(\tau,\gamma)=\begin{cases}\Omega_{p_{11}}=\{(\tau,\gamma):\tau\in[0.38,0.62],\gamma\in[50,160]\text{Hz}\}\\ \Omega_{p_{12}}=\{(\tau,\gamma):\tau\in[0,1],\gamma\in[8,26]\text{Hz}\}\end{cases} \tag{44}$$

$$Tp_2(\tau,\gamma)=\begin{cases}\Omega_{p_{21}}=\{(\tau,\gamma):\tau\in[0.55,0.77],\gamma\in[40,120]\text{Hz}\}\\ \Omega_{p_{22}}=\{(\tau,\gamma):\tau\in[0,1],\gamma\in[8,26]\text{Hz}\}\end{cases} \tag{45}$$

where the regions of support include the bands where the amplitude of TFRs is greater or equal to 1% of its maximum amplitude.

The time–frequency transformations of these two templates reveal that the transients have some overlapping time and frequency bands as shown in the two middle graphs in Fig. 4. In order to form the mutual exclusive templates $p_1'(t)$ and $p_2'(t)$, the shared time–frequency areas are excluded by windowing and the inverse time–frequency transforms are shown in the bottom two graphs of Fig. 4.

In order to test the proposed method, 10 000 test signals, $s_i(t)$, where $i=1,\ldots,10\,000$, were constructed according to (30) and (31); with half of the signals containing the patterns similar to $p_1(t)$ and the other half similar to $p_2(t)$. Both groups of signals also have the low-frequency content that is present in the original templates $p_1(t)$ and $p_2(t)$. The signals that are similar to $p_1(t)$ contain the transients in the region of $\Omega_{p_{11}}$ and the signals that are similar to $p_2(t)$ contain the transients in the region of $\Omega_{p_{21}}$. Also, they contain other transients outside the bands of the templates which further increase the degree of difficulty in classification.

Since each of these signals can contain either of the templates, a window function is needed to capture all the variations. The window $W_{\text{gd}}(\tau,\gamma)$ is designed to support the region $\Omega_{\text{gd}}=\{(\tau,\gamma):\tau\in[0.38,0.77],\quad \gamma\in[40,160]\text{Hz}\}$. Each TFR is multiplied by $W_{\text{gd}}(\tau,\gamma)$ and the inverse representations of the signals $s_i'(t)$ are obtained by using (9).

The correlations are performed by using general correlation procedure [$p_j(t)$ and $s_i(t)$] and the SRC procedure [$p_j'(t)$ and $s_i'(t)$], and the results are presented in Table I. These results represent an average of 10 000 trials.

From Table I, it can be seen clearly that the SRC performs significantly better than general correlation, especially when ST and STFT are used. The last column of Table I presents the EP. It can be concluded that the SRC-based classifier has a very high accuracy in comparison to the general correlation-based classifier. The EP for the SRC-based classifier is 0%–2% while for the conventional classifier is almost 20%.

In order for a pattern recognition scheme to be useful in practice, it should possess a high degree of sensitivity to the template, and be robust to slight variations in the signals being analyzed. The robustness of the proposed scheme is examined by stretching and shrinking the signals at three different

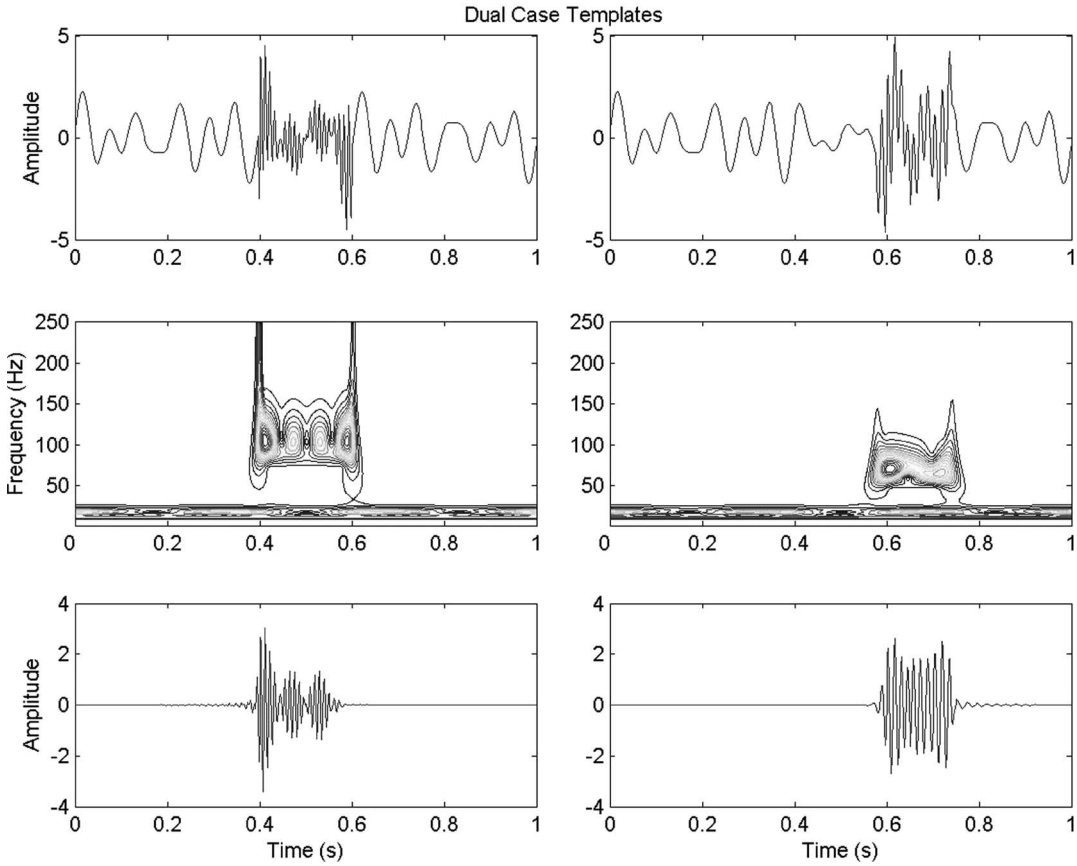

Fig. 4. Templates and (top) their time-domain representations, (middle) time–frequency domain representations, and (bottom) time domain after processing for dual case.

TABLE I
COMPARISON OF THE PEAK CORRELATION COEFFICIENT FOR SRC AND GENERAL CORRELATION

Method		ρ_M	ρ_{NM}	φ	EP
SRC	STFT	0.5827	0.0823	0.5004	0.0001%
	CWT	0.4856	0.3207	0.1649	1.9600%
	S-transform	0.5835	0.0789	0.5046	0.0000%
General Correlation		0.6127	0.5625	0.0502	19.4900%

TABLE II
ROBUSTNESS OF THE PROPOSED SCHEME TO EXPANSION AND COMPRESSION

Amount of the expansion and compression				
	0%	10%	15%	20%
ρ_M	0.5835	0.5064	0.4057	0.2834
ρ_{NM}	0.0789	0.0848	0.1197	0.1611
φ	0.5046	0.4215	0.2860	0.1223
EP	0.0000%	0.0000%	0.0002%	7.7400%

percentage points. Table II depicts the results that represent the average of 10 000 trials based on ST. Also, each trial represents the mean value of the two operations: expansion and compression.

The results of the robustness analysis clearly show that slight variations in the range of 0%–15% would have no significant effect on the performance of the pattern classifier since the accuracy remains almost the same, even though the resolution has decreased by a factor of half. However, for variations larger than 20%, deterioration in performance begins to occur. Therefore, the SRC can be considered quite robust.

D. Multiple Templates

In the case of multiple templates, the similar procedure as for dual-template case has been used. However, the task is to differentiate among four types of different signals. Again, it has been assumed that the templates have same low-frequency content but different transient features as defined in (33)–(36). The TFRs of these templates, obtained according to (1) and (22), can be summarized by the following equations:

$$Tp_1(\tau,\gamma)=\begin{cases}\Omega_{p_{11}}=\{(\tau,\gamma):\tau\in[0.38,0.62],\gamma\in[70,150]\text{Hz}\}\\ \Omega_{p_{12}}=\{(\tau,\gamma):\tau\in[0,1],\gamma\in[8,26]\text{Hz}\}\end{cases} \tag{46}$$

$$Tp_2(\tau,\gamma)=\begin{cases}\Omega_{p_{21}}=\{(\tau,\gamma):\tau\in[0.55,0.76],\gamma\in[35,75]\text{Hz}\}\\ \Omega_{p_{22}}=\{(\tau,\gamma):\tau\in[0,1],\gamma\in[8,26]\text{Hz}\}\end{cases} \tag{47}$$

$$Tp_3(\tau,\gamma)=\begin{cases}\Omega_{p_{31}}=\{(\tau,\gamma):\tau\in[0.15,0.43],\gamma\in[60,125]\text{Hz}\}\\ \Omega_{p_{32}}=\{(\tau,\gamma):\tau\in[0,1],\gamma\in[8,26]\text{Hz}\}\end{cases} \tag{48}$$

$$Tp_4(\tau,\gamma)=\begin{cases}\Omega_{p_{41}}=\{(\tau,\gamma):\tau\in[0.23,0.48],\\ \qquad\qquad\gamma\in[110,210]\text{Hz}\}\\ \Omega_{p_{42}}=\{(\tau,\gamma):\tau\in[0,1],\gamma\in[8,26]\text{Hz}\}\,.\end{cases} \tag{49}$$

However, these templates have some overlaps in the time–frequency domain as illustrated in Fig. 5. To properly

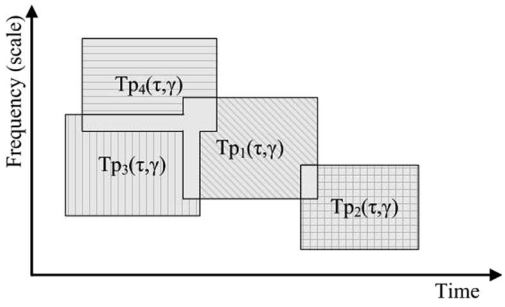

Fig. 5. Hypothetical multiple-template position.

TABLE III
COMPARISON OF THE PEAK CORRELATION COEFFICIENT FOR SRC AND GENERAL CORRELATION IN MULTIPLE-TEMPLATE CASE

Method	ρ_M	ρ_{NM}	φ	EP
SRC S-transform	0.6234	0.0988	0.5246	0.0000%
General Correlation	0.9843	0.9024	0.0819	67.2600%

develop the mutually exclusive templates, $p_i'(t)$, where $i = 1, \ldots, 4$, the shared features have to be removed from each of the four templates.

As in the case of dual templates, 10 000 test signals, generated according to (37)–(40), are used in simulation and for the time–frequency preprocessing, ST is selected. The test signals with equal probability can contain any of the templates. Table III summarizes the results of the evaluation. The advantage of SRC over the general correlation-based scheme is rather clear. The SRC not only improves the resolution, but also significantly reduces the EP. The EP for the SRC is 0%, while the EP for general correlation is 67.26%.

V. ILLUSTRATIVE EXAMPLE

A. Heart-Sound Classification by SRC Scheme

A heart malfunction, known as mitral stenosis, is often manifested through the heart sound known as the OS. This is a short sharp sound occurring in early diastole, caused by abrupt halting in its maximal opening of an abnormal atrioventricular valve [21], [22]. However, the difficulty, as shown in the top two graphs of Fig. 6, lies in the fact that the OS sounds very similar to the third heart sound (S3), which is often present in normal children or young adults. But, when it is heard in individuals over the age of 40, it usually reflects cardiac disease characterized by ventricular dilatation, decreased systolic function, and elevated ventricular diastolic filling pressure [23]–[26]. It is generally difficult to distinguish these two sounds just by listening without going through sufficient training [23].

The objective of this study is to apply the proposed technique to distinguish both conditions through pattern classification.

Thirty two phonocardiograph recordings of actual heart sounds were obtained from patients at St. Joseph's Hospital in Toronto, Canada, during clinical examinations which also included heart auscultation. Fourteen of the signals were known to contain the OS, and the remaining 18 signals contained the third heart sound. The data-acquisition system consists of an analog recorder/player (Cambridge AVR-I which was specially designed for heart sounds) and a personal computer fitted with a 16-bit acquisition board. The heart sounds are sampled at 4000 Hz for 4096 samples (1.024 s in length) [18]. The sampling rate is high enough since the maximum-frequency content of heart sounds is usually below 600 Hz [23].

TABLE IV
HEART-SOUND CLASSIFICATION BY THE SRC

Method		ρ_M	ρ_{NM}	φ	EP
SRC	STFT	0.5533	0.2413	0.3120	10.00%
	CWT	0.6731	0.5248	0.1483	16.67%
	S-transform	0.4905	0.1661	0.3244	6.670%
General Correlation		0.3477	0.3352	0.0126	56.67%

For the time–frequency analysis, three different transforms are used as outlined in Section IV. A Gaussian window with a length of 256 points is used for the STFT. A Gaussian mother wavelet is used for the CWT. A Gaussian window is also used [9] in the calculation of ST. An example of the TFR is shown in the middle two graphs of Fig. 6, which is the ST of the top two signals.

For the purpose of easy illustration, one signal from each group is selected as the template for that group and both templates are depicted in the top two graphs of Fig. 6. As shown, most of the energy associated with an OS is concentrated between 50 and 300 Hz, while that of S3 lies between 30 and 150 Hz (shaded regions in Fig. 6). Since there is an overlap in some frequency ranges between the two signals, the templates have to be decoupled. Based on the numerical analysis, it is concluded that the template for the OS $p_{\mathrm{OS}}(t)$ should have frequencies between 120 and 300 Hz and its time duration should be 50 ms, while the template for the S3 $p_{\mathrm{S3}}(t)$ should have frequencies between 30 and 70 Hz and its time duration should be 100 ms. Since the signal being analyzed could contain either an OS or an S3, the selected frequency band for the window in (7) is chosen as $\gamma \in [30\ 300]$Hz.

For classification between the OS and the S3, the OS is usually slightly closer to S2 than S3, as observed in Fig. 6 [24]. Once the relevant portions of the signal are extracted from the recordings, inverse time–frequency transforms, given by (9), can be used to convert only the relevant portions of the signal to the time domain to calculate the correlation and to carry out diagnostic decisions.

B. Results

The performance of the proposed scheme when applied to heart-sound classification is evaluated by comparing it with the general correlation, and the results are shown in Table IV. These results represent the average of thirty trials. A comparison of the values of these two states shows that the SRC performs significantly better than the general correlation.

The results in Table IV have also confirmed the speculations of earlier work [18], [19] that the ST is a superior method for the time–frequency analysis of the heart sounds to STFT and CWT. Table IV illustrates the SRC with the ST results in the peak correlation coefficient. When a match is present, the value is almost three times greater than that when there is no match. This ratio is the highest among all time–frequency analysis techniques considered.

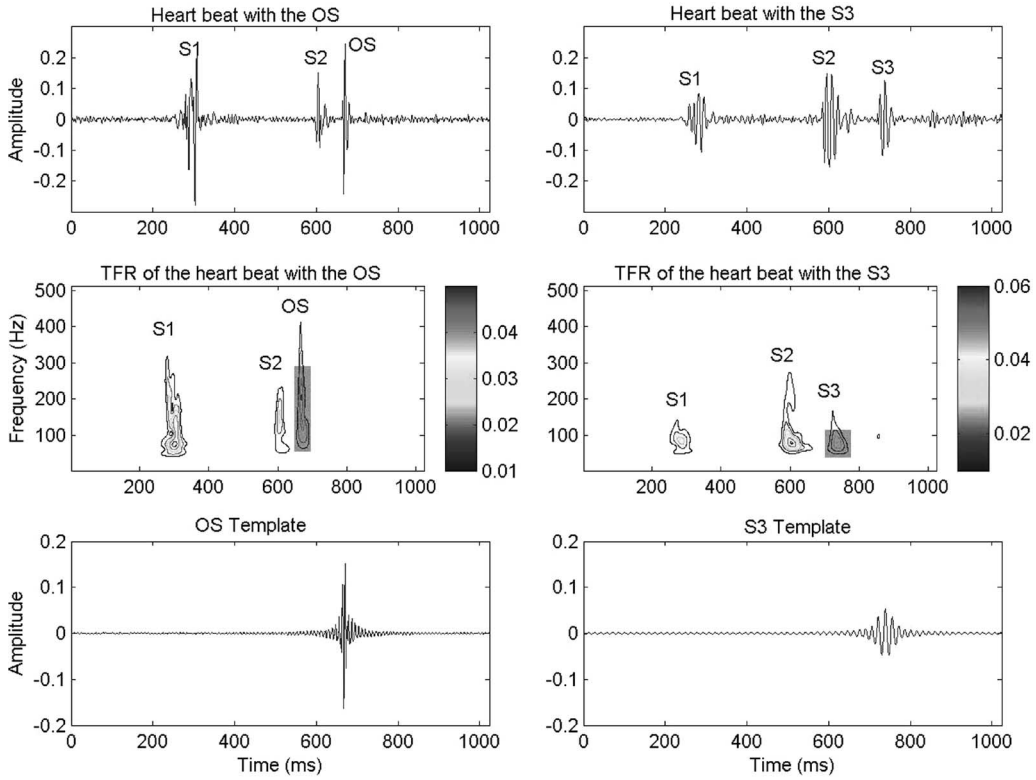

Fig. 6. Time domain, time–frequency domain representations, and the templates.

C. Remarks

1) Based on the results presented in this paper, it is clear that the proposed scheme is very encouraging. The redundant representation of a 1-D signal in a 2-D time–frequency domain can provide an additional degree of freedom for signal analysis. Even though the proposed technique is simple in principle and operation, it has significant implications in pattern recognition and other signal processing applications. One of the major concerns for the proposed scheme might be the computational complexity associated with the forward and backward time–frequency transforms. However, by the very nature of selected regions, resulting signal space has been reduced considerably.
2) Since the intent of this paper is to explore the redundancy in a 2-D representation of a 1-D signal, only a selected portion of the signal is matched against the template. However, if the template cannot be represented (or approximated) in a bandlimited form, the power of the method could be affected. In practice, however, all discrete signals and templates are bandlimited (Nyquist sampling criteria).
3) The two potential limitations of the proposed scheme are that there should be *a priori* knowledge about the phenomenon that is being classified, and in the case of the multiple templates, the overlapping bands should not contain significant features of any of the patterns. The first limitation implies that in order to use the SRC, there should be enough knowledge about the pattern, so that the template can be chosen correctly. The second limitation implies that for the multiple templates, the significant features of each pattern should not lie in the overlapped regions, otherwise, the proposed methodology may not perform satisfactory, but this is true for any pattern recognition-based technique.
4) It currently takes between 1.05 and 1.25 s as measured in MATLAB on a PC (1.39-GHz AMD Athlon processor with 256 MB of RAM) to classify whether a heart beat contains OS or S3. Therefore, the automated algorithm for heart-sound classification can be developed based on the SRC and simultaneous recording of phonocardiograph and ECG. If an ECG signal is recorded simultaneously, it can be used as a trigger signal [22]. The simultaneous recording of the ECG and the heart sounds can be very easily done with a SimulScope III from Cardionics Inc., Webster, TX.
5) The SRC can potentially be applied to many other applications where the classification of short-duration transients is required. These applications come from different areas ranging from biomedical signals [7], [27], [28] to analysis of mechanical and electrical signals [29]–[31].

VI. Conclusion

In this paper, a new technique for pattern classification based on time–frequency decomposition is developed. The correlation between the observed signal and the template is conducted only in selected regions of interest in time–frequency domain. Three time–frequency decomposition techniques have been considered: the STFT, CWT, and ST. To illustrate the performance of

the technique clearly, both mathematical analysis and numerical tests on synthetic signals have been carried out. The results have indicated conclusively that the proposed technique provides a consistent improvement over the traditional correlation-based schemes. In particular, it has been shown that the ST leads to the best overall performance. Furthermore, the proposed technique has also been applied to classification of two pathological states of heart patients by analyzing heart sounds. The scheme is capable of distinguishing the opening snaps from the third heart sound with an EP of only 6.670%.

APPENDIX I

The proof of the Theorem 1 is presented in this section. Let (8) represent the signal $s(t)$ and its composition. Assuming that $s_1(t)$ is similar to the pattern $p(t)$, and $s_2(t)$ lies in the frequency and the time bands outside those of the pattern $p(t)$

$$\left|\int_{-\infty}^{\infty} s_1(t)p(t)dt\right| \gg \left|\int_{-\infty}^{\infty} s_2(t)p(t)dt\right|. \tag{50}$$

The left-hand side of (10) is equal to

$$\max\left[\left|\operatorname{corr}\left(s_1(t),p(t)\right)\right|\right] = \max_{\tau}\left[\left|\frac{\int_{-\infty}^{\infty} s_1(t)p(t+\tau)dt}{\sqrt{\int_{-\infty}^{\infty} s_1(t)^2dt}\sqrt{\int_{-\infty}^{\infty} p(t)^2dt}}\right|\right]. \tag{51}$$

The right-hand side of (10) is equal to

$$\max\left[\left|\operatorname{corr}\left(s(t),p(t)\right)\right|\right] = \max_{\tau}\left[\left|\frac{\int_{-\infty}^{\infty} s_1(t)p(t+\tau)dt+\int_{-\infty}^{\infty} s_2(t)p(t+\tau)dt}{\sqrt{\int_{-\infty}^{\infty} s(t)^2dt}\sqrt{\int_{-\infty}^{\infty} p(t)^2dt}}\right|\right] \tag{52}$$

where

$$s(t)^2 = s_1(t)^2 + 2s_1(t)s_2(t) + s_2(t)^2. \tag{53}$$

Since

$$\sqrt{\int_{-\infty}^{\infty} s_1(t)^2dt}\sqrt{\int_{-\infty}^{\infty} p(t)^2dt} < \sqrt{\int_{-\infty}^{\infty} s(t)^2dt}\sqrt{\int_{-\infty}^{\infty} p(t)^2dt} \tag{54}$$

it follows that

$$\left|\frac{\int_{-\infty}^{\infty} s_1(t)p(t+\tau)dt}{\sqrt{\int_{-\infty}^{\infty} s_1(t)^2dt}\sqrt{\int_{-\infty}^{\infty} p(t)^2dt}}\right| > \left|\frac{\int_{-\infty}^{\infty} s_1(t)p(t+\tau)dt}{\sqrt{\int_{-\infty}^{\infty} s(t)^2dt}\sqrt{\int_{-\infty}^{\infty} p(t)^2dt}}\right|. \tag{55}$$

Hence

$$\max\left[\left|\operatorname{corr}\left(s_1(t),p(t)\right)\right|\right] > \max\left[\left|\operatorname{corr}\left(s(t),p(t)\right)\right|\right]. \tag{56}$$

APPENDIX II

The proof of Theorem 2 is presented below. Assume that there are two templates $p(t)$ and $p_1(t)$ with their time–frequency transforms defined as follows:

$$Tp(\tau,\gamma) \quad \forall \quad \tau\in[\tau_1,\tau_2] \quad \gamma\in[\gamma_2,\gamma_4] \tag{57}$$

$$Tp_1(\tau,\gamma) \quad \forall \quad \tau\in[\tau_1,\tau_2] \quad \gamma\in[\gamma_1,\gamma_3] \tag{58}$$

with $\gamma_1<\gamma_2<\gamma_3<\gamma_4$. Using the decomposition presented earlier in Corollary 2, $p(t)$ can be decomposed into two parts:

$$\begin{aligned} p(t) &= p'(t)+p''(t) \\ &= \int_{-\infty}^{\infty}\int_{-\infty}^{\infty}\left\{Tp(\tau,\gamma)-\left(Tp(\tau,\gamma)\cap Tp_1(\tau,\gamma)\right)\right\}W(\tau,\gamma) \\ &\quad\times K(\tau,\gamma,t)d\tau d\gamma+\int_{-\infty}^{\infty}\int_{-\infty}^{\infty}\left\{Tp(\tau,\gamma)\cap Tp_1(\tau,\gamma)\right\} \\ &\quad\times W(\tau,\gamma)K(\tau,\gamma,t)d\tau d\gamma. \end{aligned} \tag{59}$$

Therefore, if $z(t)$ is similar to $p_1(t)$ but different from the $p(t)$, it can be stated that its time–frequency transform is equal to

$$Tz(\tau,\gamma) \quad \forall \quad \tau\in[\tau_1,\tau_2] \quad \gamma\in[\gamma_1,\gamma_3]. \tag{60}$$

Therefore, the left side of (19) becomes

$$\max\left[\left|\operatorname{corr}\left(z(t),p(t)\right)\right|\right] = \max_{\tau}\left[\left|\frac{\int_{-\infty}^{\infty} z(t)p'(t+\tau)dt+\int_{-\infty}^{\infty} z(t)p''(t+\tau)dt}{\sqrt{\int_{-\infty}^{\infty} p(t)^2dt}\sqrt{\int_{-\infty}^{\infty} z(t)^2dt}}\right|\right] \tag{61}$$

where

$$p(t)^2 = p'(t)^2 + 2p'(t)p''(t) + p''(t)^2. \tag{62}$$

The right-hand side is equal to

$$\max\left[\left|\operatorname{corr}\left(z(t),p'(t)\right)\right|\right] = \max_{\tau}\left[\left|\frac{\int_{-\infty}^{\infty} z(t)p'(t+\tau)dt}{\sqrt{\int_{-\infty}^{\infty} p'(t)^2dt}\sqrt{\int_{-\infty}^{\infty} z(t)^2dt}}\right|\right]. \tag{63}$$

Keeping in mind the mutual exclusivity of the templates and the constraint imposed by Corollary 2, it can be concluded that

$$\left|\int_{-\infty}^{\infty} z(t)p''(t+\tau)dt\right| \gg \left|\int_{-\infty}^{\infty} z(t)p'(t+\tau)dt\right| \quad (64)$$

$$\sqrt{\int_{-\infty}^{\infty}\left\{p'(t)^2+2p'(t)p''(t)+p''(t)^2\right\}dt} \approx \sqrt{\int_{-\infty}^{\infty} p'(t)^2dt}. \quad (65)$$

Using (64) and (65), (19) is established

$$\max\left[\left|\mathrm{corr}\left(z(t),p(t)\right)\right|\right] > \max\left[\left|\mathrm{corr}\left(z(t),p'(t)\right)\right|\right]. \quad (66)$$

ACKNOWLEDGMENT

The authors would like to thank G. Livanos and N. Ranganathan for their valuable inputs regarding heart sounds, and the anonymous reviewers for their comments regarding the manuscript. Their comments have helped tremendously improve the technical quality and the presentation of the manuscript.

REFERENCES

[1] D. Kil and F. Shin, *Pattern Recognition and Prediction With Applications to Signal Characterization*. Woodbury, NY: AIP Press, 1996.
[2] M. Akay, *Detection and Estimation Methods for Biomedical Signals*. San Diego, CA: Academic, 1996.
[3] K. Grochenig, *Foundations of Time-Frequency Analysis*. Boston, MA: Birkhauser, 2001.
[4] L. Cohen, *Time-Frequency Analysis*. Englewood Cliffs, NJ: Prentice-Hall, 1995.
[5] I. Daubechies, *Ten Lectures on Wavelets*. Philadelphia, PA: SIAM, 1992.
[6] S. Mallat, *A Wavelet Tour of Signal Processing*, 2nd ed. San Diego, CA: Academic, 1999.
[7] M. Akay, Ed., *Time-Frequency and Wavelets in Biomedical Signal Processing*. Piscataway, NJ: IEEE Press, 1998.
[8] A. Akansu and R. Haddad, *Multiresolution Signal Decomposition: Transforms, Subbands, and Wavelets*. San Diego, CA: Academic, 2001.
[9] R. Stockwell, L. Mansinha, and R. Lowe, "Localization of the complex spectrum: The S-transform," *IEEE Trans. Signal Process.*, vol. 44, no. 4, pp. 998–1001, Apr. 1996.
[10] W. Chou and B. H. Juang, Eds., *Pattern Recognition in Speech and Language Processing*. London, U.K.: CRC, 2003.
[11] J. Jiang, "Design of reconfigurable control systems using eigenstructure assignments," *Int. J. Control*, vol. 59, no. 2, pp. 395–410, 1994.
[12] J. L. Blue, G. T. Candela, P. J. Grother, R. Chellappa, C. L. Wilson, and J. D. Blue, "Evaluation of pattern classifiers for fingerprint and OCR applications," *Pattern Recognit.*, vol. 27, no. 4, pp. 485–501, Apr. 1994.
[13] A. Milosavljević, "Algorithmic significance, mutual information, and DNA sequence comparisons," in *Proc. Data Compress. Conf.*, Mar. 29–31, 1994, p. 457.
[14] P. Moreels and S. E. Smrekar, "Watershed identification of polygonal patterns in noisy SAR images," *IEEE Trans. Signal Process.*, vol. 12, no. 7, pp. 740–750, Jul. 2003.
[15] R. Shiavi, *Introduction to Applied Statistical Signal Analysis*, 2nd ed. San Diego, CA: Academic, 1999.
[16] L. L. Scharf, *Statistical Signal Processing: Detection, Estimation, and Time Series Analysis*. Reading, MA: Addison-Wesley, 1991.
[17] *Two-Dimensional Digital Signal Processing I: Linear Filters*, T. Huang, Ed. New York: Springer-Verlag, 1981.
[18] G. Livanos, N. Ranganathan, and J. Jiang, "Heart sound analysis using the S-transform," in *Proc. Comput. Cardiol.*, Cambridge, MA, Sep. 24–27, 2000, pp. 587–590.
[19] M. Varanini, G. D. Paolis, M. Emdin, A. Macerata, S. Pola, M. Cipriani, and C. Marchesi, "Spectral analysis of cardiovascular time series by the S-transform," in *Proc. Comput. Cardiol.*, Lund, Sweden, Sep. 7–10, 1997, pp. 383–386.
[20] R. Pinnegar, "The generalized S-transform and TT-transform, in one and two dimensions," Ph.D. dissertation, Univ. Western Ontario, London, ON, Canada, Sep. 2001.
[21] E. Horovitz, *Heart Beat: A Complete Guide to Understanding and Preventing Heart Disease*. Los Angeles, CA: Health Trend Publishing, 1988.
[22] M. G. Khan, *Heart Disease Diagnosis and Therapy: A Practical Approach*. Baltimore, MD: Williams & Wilkins, 1996.
[23] A. Ravin, *Auscultation of the Heart*, 3rd ed. Chicago, IL: Year Book Medical, 1977.
[24] B. Erickson, *Heart Sounds and Murmurs: A Practical Guide*, 3rd ed. St. Louis, MO: Mosby-Year Book, 1997.
[25] M. Obadiat, "Phonocardiogram signal analysis: Techniques and performance analysis," *J. Med. Eng. Technol.*, vol. 17, no. 6, pp. 221–227, Nov./Dec. 1993.
[26] L. Durand and P. Pibarot, "Digital signal processing of the phonocardiogram: Review of the most recent advancements," *Crit. Rev. Biomed. Eng.*, vol. 23, no. 3/4, pp. 169–219, 1995.
[27] H. S. Liu, T. Zhang, and F. S. Yang, "A multistage, multimethod approach for automatic detection and classification of Epileptiform EEG," *IEEE Trans. Biomed. Eng.*, vol. 49, no. 12, pp. 1557–1566, Dec. 2002.
[28] H. Chan, H. Huang, and J. Lin, "Time-frequency analysis of heart rate variability during transient segments," *Ann. Biomed. Eng.*, vol. 29, no. 11, pp. 983–996, Nov. 2001.
[29] A. G. Rehorn, E. Sejdić, and J. Jiang, "Fault diagnosis in machine tools using selective regional correlation," *Mech. Syst. Signal Process.*, vol. 20, no. 5, pp. 1221–1238, Jul. 2006.
[30] W. J. Staszewski, K. Worden, and G. R. Tomlinson, "Time-frequency analysis in gearbox fault detection using the Wigner-Ville distribution and pattern recognition," *Mech. Syst. Signal Process.*, vol. 11, no. 5, pp. 673–692, Sep. 1997.
[31] P. Purkait and S. Chakravorti, "Pattern classification of impulse faults in transformers by wavelet analysis," *IEEE Trans. Dielectr. Electr. Insul.*, vol. 9, no. 4, pp. 555–561, Aug. 2002.

Ervin Sejdić (S'00) received the B.E.Sc. degree in electrical engineering with a specialization in wireless communications from the University of Western Ontario, London, ON, Canada, in 2002, where he is currently working toward the Ph.D. degree in electrical engineering.

His research interests include digital signal processing, system identification, general time–frequency analysis, and adaptive filtering for both biomedical and mechanical applications.

Mr. Sejdić won prestigious research scholarships from the Natural Sciences and Engineering Research Council of Canada in 2003 and 2005.

Jin Jiang (S'85–M'87–SM'94) received the B.E.Sc. degree from Xi'an Jiaotong University, Xi'an, China, in 1982, and the M.E.Sc. and Ph.D. degrees from the University of New Brunswick, Fredericton, NB, Canada, in 1984 and 1989, respectively.

Since 1991, he has been with the University of Western Ontario, London, ON, Canada, where he is currently a Professor with the Department of Electrical and Computer Engineering. He has wide range of research interests, including fault-tolerant control of safety-critical systems (aircraft, nuclear power plants), advanced control of electrical power plants and power systems (combustion, generation, transmissions, and fuel cells), and advanced signal processing for diagnosis applications (manufacturing processes and human hearts). He has published extensively in the above areas including a recent book on active fault-tolerant control systems.

Dr. Jiang has been an NSERC/UNENE Senior Industrial Research Chair in the area of control, instrumentation, and electrical systems in nuclear power plants since 2003.